PCCP

Acid–base properties of $Cu_{1-x}Co_xFe_2O_4$ ferrospinels: FTIR investigations

Thomas Mathew, Balkrishna B. Tope, N. R. Shiju, Sooryakant G. Hegde, Bollapragada S. Rao and Chinnakonda S. Gopinath*

Catalysis Division, National Chemical Laboratory, Dr. Homi Bhabha Road, Pune 411 008, India. E-mail: gopi@cata.ncl.res.in

Received 2nd May 2002, Accepted 24th June 2002
First published as an Advance Article on the web 30th July 2002

Systematic IR spectroscopic studies were undertaken to investigate the acid–base properties of Cu–Co ferrospinels $Cu_{1-x}Co_xFe_2O_4$ ($x = 0$ to 1) employed in phenol methylation to produce 2,6-xylenol. The IR spectra of the ferrospinels reveal that Fe^{3+} and Co^{2+} ions are mainly responsible for the various hydroxy groups on the surface. Temperature dependent IR studies of pyridine adsorbed on spinels and on the spinel phase with deliberately added metal oxide exemplify the contribution of the metal ions and their coordination state towards Lewis acidity. IR studies of the spinel surface with adsorbed CO_2 and adsorption studies of electron acceptors such as 7,7,8,8-tetracyanoquinodimethane, 2,3,5,6-tetrachloro-1-4-benzoquinone and *p*-dinitrobenzene were carried out to evaluate the nature of the basic sites and the strength and distribution of the electron donor sites present on the spinel surface. It was found that the acidity (basicity) of the $Cu_{1-x}Co_xFe_2O_4$ spinel system increases (decreases) from $x = 0$ to 1. A correlation between acidity, basicity and catalytic performance reveals that an intermediate acid–base character enhances the phenol methylation activity.

1. Introduction

Among spinels, ferrites having a general formula MFe_2O_4 (where 'M' is a divalent metal such as Mg, Cu, Co, Zn, Fe, Mn *etc.*) have been used in recent years as aromatic alkylation catalysts.[1–6] Ferrites used in catalytic applications are generally synthesized by low temperature co-precipitation methods[1–6] which overcome the drawbacks such as low surface area, varying morphology, inhomogeneity at an atomistic level and large particle with grain boundary, generally associated with high temperature preparation.[7] Further, co-precipitation methods generate Brønsted acid sites in different cationic environments in addition to Lewis sites, which makes the catalyst active and effective for many organic transformations such as aromatic alkylation, acylation *etc.*[2–4,6] Identification of these Lewis and Brønsted acid sites is an important task in understanding the surface states of ferrospinels, which in turn will be useful in understanding the mode of adsorption of organic molecules and thereby the reaction mechanism on the surface. A variety of physicochemical methods have been applied to evaluate the strength and the amount of acid–base sites on catalysts and a large variety of probe molecules have been utilized.[8–11] When pyridine is chemisorbed on a surface possessing acid properties, it can interact with acidic protons, electron acceptor sites and H from neutral or weakly acidic hydroxy groups.[12,13] However, CO_2 has been used to probe basic surface properties due to its amphoteric character (also known for its acidic nature) and hence it is expected to adsorb on both acidic and, more strongly, on basic sites.[14,15] On the other hand, adsorption of electron acceptor (EA) molecules like 7,7,8,8-tetracyanoquinodimethane (TCNQ), 2,3,5,6-tetrachloro-1-4-benzoquinone (chloranil) and *p*-dinitrobenzene (PDNB) on the oxide surface will provide insight into the strength and distribution of electron donor sites on the oxide surfaces.[16,17] By probing the interaction of all the above molecules adsorbed on the ferrospinel surface, information can be obtained about the oxidation state of the metal ion, the coordination symmetry, the degree of coordination unsaturation of the surface hydroxy groups and the nature of surface Lewis and Brønsted acid sites.[12]

Transition metal oxides are primarily redox catalysts and not much work has been done on investigating their acid–base properties. Although both acidic and basic sites exist on transition metal oxides, these are generally classified as acidic oxides or A-type oxides, as described by Auroux and Gervasini.[18] For oxides like ferrospinel, the acid–base properties can be decisive in determining their catalytic activity.

In a continuing study of aromatic alkylation using different ferrospinels,[1–5,19,20] we report here the detailed acid–base properties of $Cu_{1-x}Co_xFe_2O_4$ using IR spectroscopy. FTIR studies have been carried out on $Cu_{1-x}Co_xFe_2O_4$ ($x = 0$ to 1) surfaces with adsorbed pyridine and CO_2 and adsorption studies of electron acceptors such as TCNQ, chloranil and PDNB. The nature of the OH groups on these catalysts and their interaction in the presence of adsorbed pyridine and CO_2 molecules are reported. The $Cu_{1-x}Co_xFe_2O_4$ surface is predominantly Lewis acid in character with a large occupancy of O_h coordinated metal ions. Acid–base properties vary linearly but in an exactly opposite manner with increasing x and an intermediate acid–base strength of $Cu_{1-x}Co_xFe_2O_4$ favours high methylation activity.

2. Experimental

$Cu_{1-x}Co_xFe_2O_4$($x = 0$, 0.25, 0.5, 0.75 and 1) samples were prepared by a co-precipitation technique and characterized by analytical techniques as described in our earlier papers.[2–4,19,20] Table 1 shows the physicochemical and textural properties. The chemical compositions of the calcined catalysts were determined by X-ray fluorescence (XRF) and found to be in line with the starting composition. X-ray diffraction (XRD)

 DOI: 10.1039/b204226f

Table 1 Chemical analysis, XRD parameter, surface area and XPS parameters of $Cu_{1-x}Co_xFe_2O_4$

	Metal concentration (wt.%)[a]								
x	Co	Cu	Fe	Crystallite size/nm	a/Å	Surface area/m^2 g^{-1}	Micropore surface area/m^2 g^{-1}	$10^{-3}\times$ Total pore volume/cm^3 g^{-1}	Fe/(Cu + Co) Surface atomic ratio from XPS
0.0	—	27.1	46.2	15.25	8.3898	28.8	3.0	51.0	0.85
0.25	6.1	20.2	46.7	13.85	8.4051	34.0	7.8	66.7	0.81
0.50	12.4	13.5	47.1	13.17	8.4012	43.8	10.2	108.6	0.90
0.75	18.6	6.9	47.3	14.77	8.3982	36.6	4.3	63.6	1.00
1.0	25.1	—	47.6	14.13	8.3997	36.8	6.9	59.4	1.33

[a] Chemical analysis results obtained from XRF.

patterns of the powder catalysts were recorded using a Rigaku Geigerflex instrument equipped with Cu-Kα radiation ($\lambda = 1.5405$ Å) with a Ni-filter. The size and morphology of the crystals of all the samples were examined using a JEOL JSM-840A scanning electron microscope. The IR spectra of the ferrite samples were recorded by a diffuse reflectance (DR) method (Shimadzu, model 8300) between 400 cm^{-1} and 1000 cm^{-1}. The BET surface area and pore volume of the catalysts were determined by a N_2 adsorption–desorption method at 77 K using a Quantachrome Nova-1200 adsorption unit (Table 1).

FTIR studies of the samples with adsorbed CO_2 and pyridine were recorded in drift mode. A calcined powder sample in a sample holder was placed in a specially designed cell. The samples were then heated *in situ* from room temperature to 673 K at a heating rate of 5 °C min^{-1} in a flowing stream (40 ml min^{-1}) of 99.99% pure N_2. The sample was kept at 673 K for 3 h and then the hydroxy region of the spectra was measured. The sample was then cooled to 373 K and pyridine vapour was introduced into the N_2 flow for 10 min. The temperature was then slowly increased under the N_2 flow and IR spectra were recorded at different temperatures up to 673 K. A resolution of 2 cm^{-1} is attained after averaging over 500 scans for all the IR spectra reported here. For CO_2 adsorption, 99.99% pure CO_2 (Linde Air) was introduced for 1 h in N_2 at a flow rate of 40 ml h^{-1} at room temperature after the *in situ* activation.

Adsorption studies with EA molecules were carried out on $Cu_{1-x}Co_xFe_2O_4$ as described in our earlier papers.[2–4] The adsorption study was carried out over 0.5 g of catalyst placed in a cylindrical glass vessel and outgassed at 1.3×10^{-3} Pa for 1 h. Subsequently, 20 ml of a solution of the EA in acetonitrile was added, and the solution was stirred at room temperature for 4 h in a thermostatted bath. The EA adsorption was measured using a UV–VIS spectrophotometer.

3. Results

3.1. General characterisation

Fig. 1(a) shows the XRD patterns of the calcined catalysts. It can be seen that the fresh Cu-rich catalyst ($x = 0.0$) exhibits a diffraction pattern attributed to the cubic spinel phase[21] and a considerable amount of unreacted CuO and Fe_2O_3 phases. This indicates that the spinel formation is not complete at 773 K for $x = 0$. Addition of Co results in the formation of a uniform structure and the additional reflections due to impurities seen in the previous case are hardly detected at $x \geqslant 0.25$. The lattice constants, a, obtained for $CuFe_2O_4$ and $CoFe_2O_4$ are 8.3898 Å and 8.3997 Å respectively, in good agreement with the literature values.[21–23] The fine particle size of the ferrite is evident from the crystallite size of 13 to 16 nm for all samples (Table 1) estimated from the most intense peak (311) using the Debye–Scherrer equation,[24]

$$D_{hkl} = 0.9\lambda/B\ \cos\theta \quad (1)$$

where D_{hkl}, λ, B and θ are the volume average particle diameter, X-ray wavelength, full width at half maximum (FWHM) and diffraction angle, respectively. Scanning electron micrographs indicate a particle size in the range 1–6 μm (results not shown) for all samples.

The results obtained from surface area analysis of $Cu_{1-x}Co_xFe_2O_4$ are summarized in Table 1. N_2 isotherms of all these compositions represent a combination of type IV and type II nature (not shown). The isotherms of type IV indicate the presence of mesopores and the diameter of the mesopore is 33 ± 0.5 Å for all the compositions, indicating a uniformity of the pores.

Fig. 1(b) shows the metal ions distributed in two different environments in spinel at 710 cm^{-1} (ν_1) and 460 cm^{-1} (ν_2) (solid arrows), attributed to tetrahedral (T_d) and octahedral (O_h) coordinated metal–oxygen bands respectively, and the phase formation can be very well assigned from the appearance of two broad DR-IR bands.[25–28] The broad absorption bands for $Cu_{1-x}Co_xFe_2O_4$ indicate the inverse nature of spinel for all the compositions. The change in the M–O bond

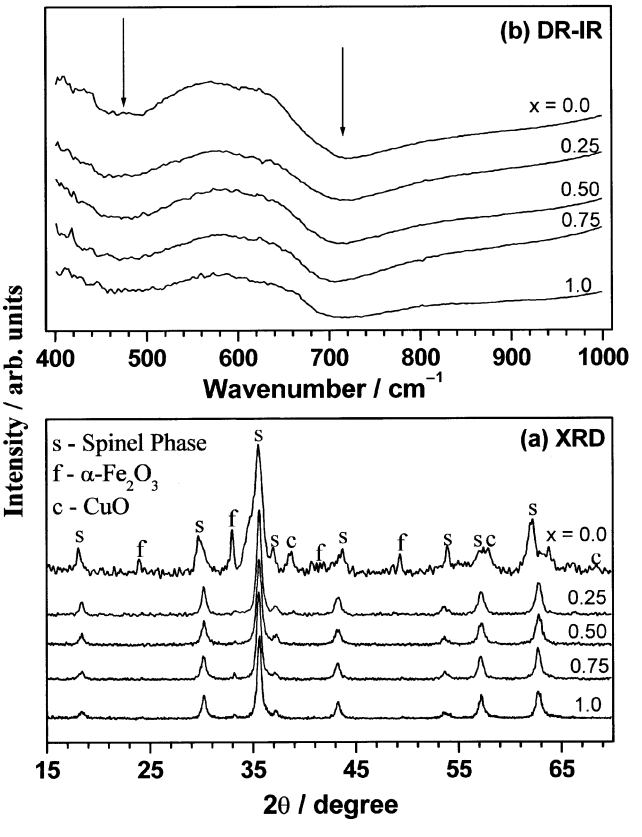

Fig. 1 (a) X-ray diffractograms and (b) DR-IR of $Cu_{1-x}Co_xFe_2O_4$ samples recorded at room temperature after calcination at 773 K. Arrows in DR-IR indicate ν_{M-O} of T_d (710 cm^{-1}) and O_h (460 cm^{-1}) coordinated cations.

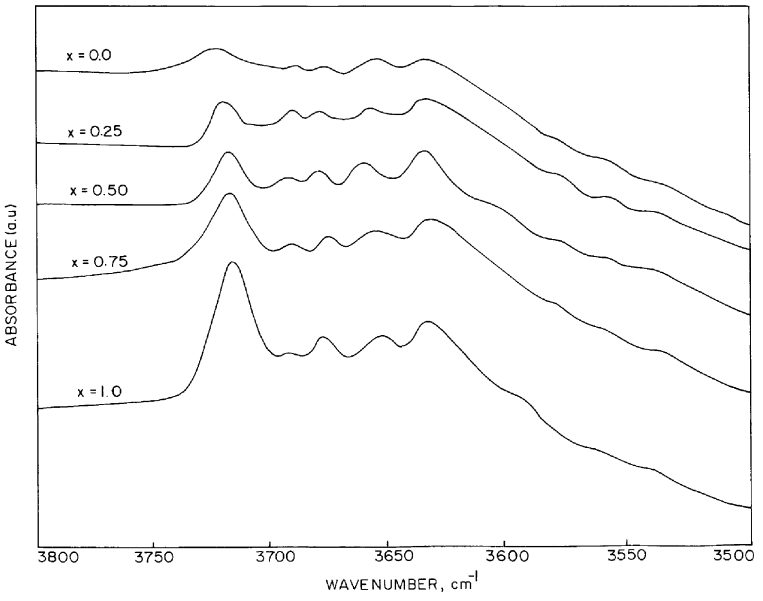

Fig. 2 FTIR spectra of OH groups on $Cu_{1-x}Co_xFe_2O_4$ after *in situ* activation at 673 K.

distances for O_h and T_d sites leads to the difference in the two band positions. According to Waldron,[27] T_d coordination bonds have the effect of substantially increasing $\nu_{cation-O}$, since these cations introduce a supplementary restoring force in a preferential direction along the M–O bond.

3.2. Hydroxy groups on $Cu_{1-x}Co_xFe_2O_4$

FTIR spectra of the surface hydroxy groups of $Cu_{1-x}Co_x$-Fe_2O_4 are presented in Fig. 2. The most intense band is found in the 3735–3710 cm^{-1} range and the intensity of the OH bands, in general, increases with increasing Co content. The above band is comprised of terminal OH over T_d coordinated Fe^{3+}, Co^{2+} and Cu^{2+} ions and coordinatively unsaturated Fe^{3+} (O_h) ion.[29–35] In addition, the spectra show broad bands centered at approximately 3695, 3680, 3660 and 3635 cm^{-1} attributed to terminal OH over O_h coordinated Fe^{3+}, Co^{2+} and Cu^{2+} ions. Many of these bands are well documented in the literature for various oxides such as γ-Fe_2O_3, α-Fe_2O_3,[29–31] $MgFe_2O_4$,[29] $ZnFe_2O_4$,[29] $CoAl_2O_4$,[32,33] CoO,[34] CuO,[35] *etc.* A relevant list of the most intense ν_{OH} bands associated with different cations having different coordination number, oxidation state and cationic environment on various oxides are presented in Table 2.

3.3. Pyridine adsorption

The IR spectrum of pyridine adsorbed on $Cu_{1-x}Co_xFe_2O_4$ at 373 K is shown in Fig. 3. Important pyridine ring modes occur at approximately 1606, 1573, 1485 and 1446 cm^{-1} termed ν_{8a}, ν_{8b}, ν_{19a} and ν_{19b} respectively[36,37] and are listed in Table 3. Note that the pyridine molecule can be retained on the surface of oxides in the following three different modes:[10] (1) interaction of the N lone pair electron and the H atom of the OH group, (2) transfer of a proton from a surface OH group to the pyridine forming a pyridinium ion (Brønsted acidity), and (3) pyridine coordination to an electron deficient metal atom (Lewis acidity). Predominant IR bands, ν_{8a} and ν_{19b}, confirm that the major contribution of acidity is due to Lewis acid sites for all compositions. Among the above four vibration modes, ν_{8a} is very sensitive with respect to the oxidation state, coordination symmetry and cationic environment.[12] A broad ν_{8a} band at 1606 cm^{-1} at $x = 0$ decreases in width at higher x values and indicates a decrease in the disorder of cation distribution in these spinels. ν_{8b} at 1575 cm^{-1} is found to be very labile and its stability on the surface is temperature dependent.[29,32] When the temperature increases above 373 K, the ν_{8b} band completely disappears, confirming its labile nature. Hence, it is concluded that these species are bound to the terminal OH groups *via* H-bonding. This coordinative

Table 2 Assignments of the bands of surface hydroxy groups on various oxide surfaces

Material	Position of ν_{OH}/cm^{-1}	Assignments	Ref.
γ-Fe_2O_3	3725	Terminal OH bonded to tetrahedral Fe^{3+}	29
	3675	Terminal OH bonded to octahedral Fe^{3+}	
	3640	Bridging OH	
α-Fe_2O_3	3720, 3680, 3635	Vibrations of three types of isolated OH group each liganded to a single Fe^{3+}	29–31
$MgFe_2O_4$	3690	Terminal OH over octahedral Fe^{3+}	29
$CoAl_2O_4$	3725	Terminal OH bonded to $_{IV}Co^{2+}$	32,33
	3580	Triply bridging OH or due to H bonded or more perturbed OH groups	
$ZnFe_2O_4$	3680	Terminal OH on tetrahedral Zn^{2+}	29
	3650	Terminal OH on octahedral Fe^{3+}	
	3610	Bridging OHs	
CuO	3690	Terminal OH	35
CoO	3680, 3658, 3639	Terminal OH	34

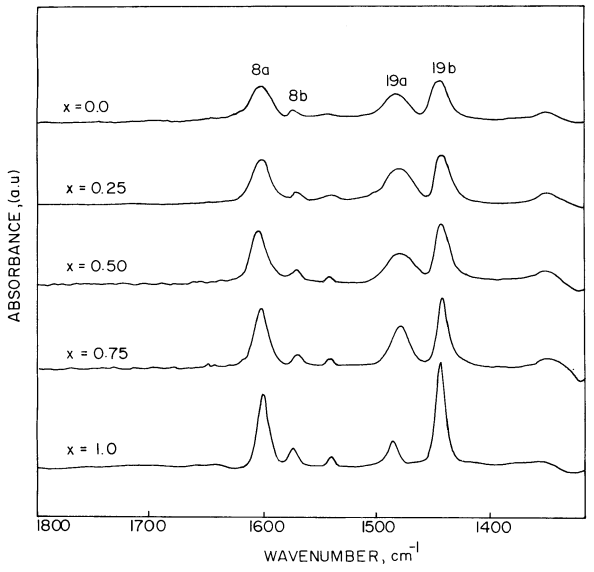

Fig. 3 FTIR spectra of $Cu_{1-x}Co_xFe_2O_4$ surfaces with adsorbed pyridine at 373 K, after *in situ* activation at 673 K.

interaction is very weak and the molecule bound in this way is desorbed at high temperature. A weak band centered at ~1540 cm^{-1} is attributed to pyridinium ion.[6,12]

3.4. Temperature dependence of pyridine adsorption

FTIR spectra of pyridine adsorbed on $Cu_{1-x}Co_xFe_2O_4$ samples were recorded between 373 K and 673 K. The results for three selected compositions, $x = 0$, 0.50 and 1 are shown in Fig. 4. Important changes in the spectral features are highlighted: (1) The bands corresponding to ν_{8a}, ν_{19a} and ν_{19b} modes display a broad and intense peak for all the compositions up to 573 K. The presence of certain pyridine bands is observed even at 673 K on $CoFe_2O_4$, in contrast to the absence of these bands on the Cu-containing samples. (2) The bands corresponding to ν_{8a} shift to higher ν as the temperature increases for all compositions. (3) ν_{19a} and ν_{19b} bands are shifted to lower ν with increasing temperature for all the compositions. An apparent single band centered at 1446 cm^{-1} at 373 K is split into two components at intermediate compositions ($0 < x < 1$) at higher temperatures. (4) For all compositions a band centered at ~1352 cm^{-1} increases in intensity as the temperature increases up to 573 K; and (5) a weak band observed at ~1541 cm^{-1} due to pyridinium ion increases in intensity and width as the temperature increases to 473 K. Fig. 5 shows the difference IR spectra of pyridine adsorbed at 373 K and the corresponding activated sample of $Cu_{1-x}Co_xFe_2O_4$. The difference spectrum shows negative bands corresponding to a lower intensity of the OH groups due to perturbation by pyridine adsorption.

Table 3 Position of the various IR bands (in cm^{-1}) of pyridine and pyridinium ion adsorbed at 373 K over various compositions of $Cu_{1-x}Co_xFe_2O_4$

Composition	ν_{8a}	ν_{8b}	$\nu_{pyridinium\ ion}$	ν_{19a}	ν_{19b}
$CuFe_2O_4$	1606	1573	1541	1485	1446
$Cu_{0.75}Co_{0.25}Fe_2O_4$	1608	1575	1541	1485	1446
$Cu_{0.5}Co_{0.5}Fe_2O_4$	1608	1573	1548	1485	1446
$Cu_{0.25}Co_{0.75}Fe_2O_4$	1608	1573	1543	1483	1446
$CoFe_2O_4$	1604	1575	1541	1487	1446

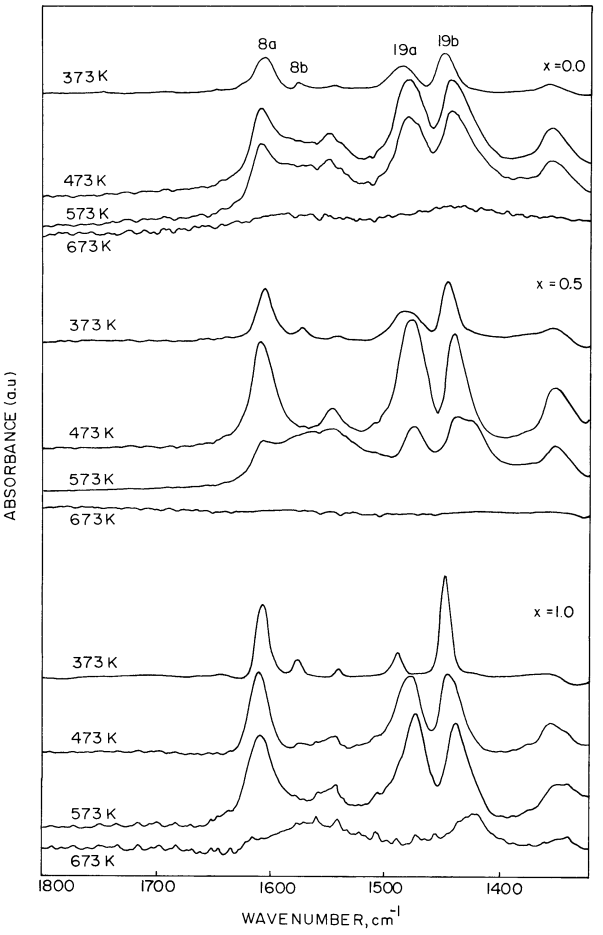

Fig. 4 Temperature dependent FTIR spectra of $Cu_{1-x}Co_xFe_2O_4$ surfaces with adsorbed pyridine for three selected compositions $x = 0$, 0.50 and 1 between 373 K and 673 K.

3.5. Basicity

3.5.1. CO_2 adsorption. The IR spectrum of CO_2 adsorbed on $Cu_{1-x}Co_xFe_2O_4$ at 298 K is shown in Fig. 6. Asymmetric stretching of adsorbed CO_2 and carbonate vibrations are observed at 2400–2300 cm^{-1} and 1800–1200 cm^{-1} respectively.[15,38–43] The IR spectrum of adsorbed CO_2 demonstrates three different types of adsorption as follows: (1) Two sharp bands are observed at 2359 and 2341 cm^{-1} (corresponding CO_2 gas phase bands[44] are at 2358 cm^{-1} and 2338 cm^{-1}) resulting from the coordination of CO_2 on the surface Lewis acid sites. CO_2 retain its linear shape with this mode of adsorption.[38,45] (2) The intensity of various bands observed between 1700 cm^{-1} and 1260 cm^{-1} (symmetric OCO stretching of bidentate and unidentate carbonates at 1430–1260 cm^{-1}, asymmetric OCO stretching of unidentate carbonate and symmetric OCO stretching of bicarbonate at 1580–1435 cm^{-1} and asymmetric OCO stretching of bicarbonate and asymmetric OCO stretching of bidentate carbonates at 1680–1600 cm^{-1})[40–43,45,46] generally decreases with increasing x, indicating a decrease in basicity from $x = 0$ to 1. (3) The width and intensity of the carbonate vibrations suggests that the bidentate mode seems to be the dominant adsorption state on $Cu_{1-x}Co_xFe_2O_4$ and indicates the presence of coordinatively unsaturated ions. The absence of other bands in the 2270–1700 cm^{-1} range suggests the absence of bridged CO_2 species on the oxide surface.

3.5.2. Adsorption studies of TCNQ and chloranil. Adsorption studies of three EAs, namely, TCNQ, chloranil and

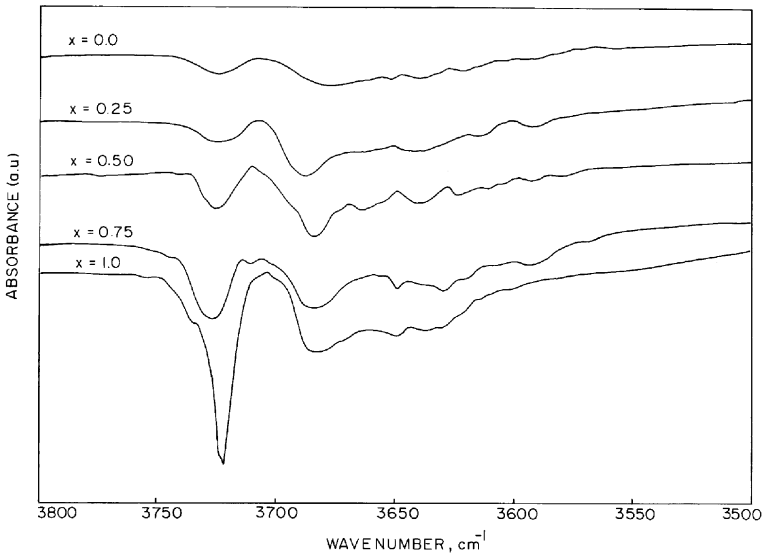

Fig. 5 Difference IR spectra of the hydroxy regions of $Cu_{1-x}Co_xFe_2O_4$ between surfaces with adsorbed pyridine and calcined surfaces at 373 K.

PDNB with electron affinity values 2.84, 2.40 and 1.77 eV, respectively, were performed on $Cu_{1-x}Co_xFe_2O_4$.[47,48] Langmuir-type adsorption isotherms obtained on catalysts activated at 500 °C are shown in Fig. 7 for (a) TCNQ, (b) chloranil and (c) the difference between TCNQ and chloranil for each composition. Since TCNQ is a strong EA it forms anion radicals upon adsorption from strong to weak donor sites. However, chloranil can accept electrons from both strong and moderately strong donor sites. Negligible adsorption of PDNB (results not shown) in all systems indicates the absence of very strong donor sites. This demonstrates that the adsorption sites on Cu–Co ferrites act as electron donors to the adsorbed molecule with electronaffinity values >1.77 eV. EA adsorption studies indicate that the basicity of the $Cu_{1-x}Co_x$-Fe_2O_4 system decreases with increasing x. The difference between the limiting amounts of TCNQ and chloranil adsorbed (Fig. 7(c)) indicates that the Cu-rich compositions possess a large number of strong and moderately strong donor sites. Nonetheless, with increasing x, the strength of the donor sites decreases.

4. Discussion

4.1. Composition dependence of hydroxy species on $Cu_{1-x}Co_xFe_2O_4$

Various OH bands seen in Fig. 2 are due to terminal and bridging OH bonded over metal ions in T_d and O_h coordination and the strength of the various OH bands is in the following order (Table 2): T_d coordinated terminal OH > O_h-coordinated terminal OH > bridging OH. Although OH groups bonded over various ions are present on the surface, the contribution from each ion towards any specific band is different in terms of intensity and strength. It is clear that, unlike CuO,[35] oxides based on iron show a variety of OH bands indicating a considerable role in the formation and stable existence of OH on the surface. Nevertheless, as the Co content increases the intensity of the various OH bands increases, indicating a direct influence on the number and strength of the surface OH groups. However, it is very difficult to isolate the contribution of each metal ion because of the large overlap of the OH bands by all the metal ions.

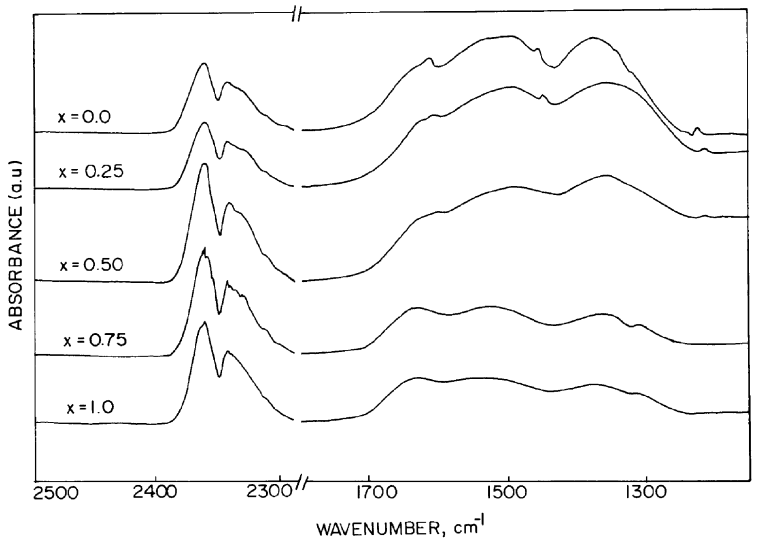

Fig. 6 FTIR spectra of CO_2 adsorbed on $Cu_{1-x}Co_xFe_2O_4$ at room temperature (298 K).

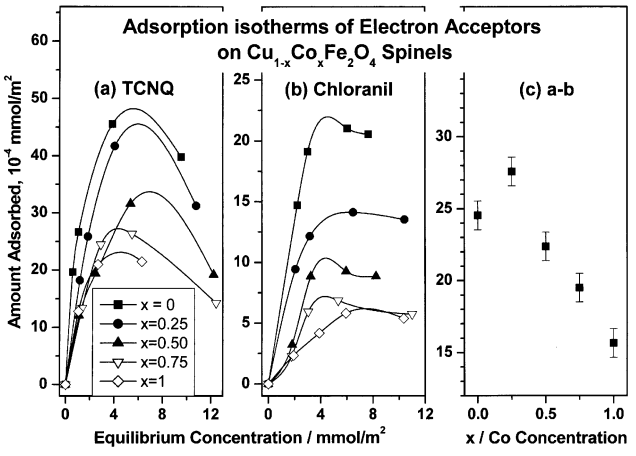

Fig. 7 Adsorption isotherms of (a) TCNQ and (b) chloranil in acetonitrile on $Cu_{1-x}Co_xFe_2O_4$ system calcined at 773 K. The difference between the limiting amounts of TCNQ and chloranil adsorbed at each composition is shown in (c).

4.2. Acidity of $Cu_{1-x}Co_xFe_2O_4$

From Table 3 and Fig. 3, it is clear that both Lewis and Brønsted acid sites are available on the $Cu_{1-x}Co_xFe_2O_4$ surfaces, but the Lewis acid sites are dominant (ν_{8a}). ν_{8a} depends on the strength of the Lewis site, which in turn depends on the type of metal, coordination number, oxidation state, redox behavior and the presence of other metal ions surrounding it.[12] The peak maximum of the ν_{8a} bands lies at 1606 ± 2 cm^{-1} for all compositions suggesting that pyridine preferentially coordinates to all transition metal ions in O_h symmetry (Table 3). This is further supported by the temperature dependent IR studies of pyridine adsorption on $CuFe_2O_4$ containing a deliberate excess of 0.5 mol CuO or 0.5 mol Fe_2O_3, where Cu^{2+} and Fe^{3+} have O_h symmetry; the results are shown in Fig. 8. This experiment was also performed with other Cu-containing compositions. Though the T_d coordinated Fe^{3+} ions are diluted by O_h ions in these systems, all the compositions exhibit a ν_{8a} band at 1606 cm^{-1}, exactly similar to $CuFe_2O_4$. Similar results were obtained with an excess of 0.5 mol CoO or 0.5 mol Fe_2O_3 with $CoFe_2O_4$ (Fig. 9). This again indicates the predominant contribution of O_h ions over T_d ions to the ν_{8a} band upon pyridine adsorption. The above conclusion is supported by the work of Jacobs *et al.*[49] using low energy ion scattering, that revealed that mainly octahedral cations are exposed on the surface of spinels. The above discussion leads to the conclusion that the contribution to pyridine adsorption of O_h cations is larger than that of T_d ions.

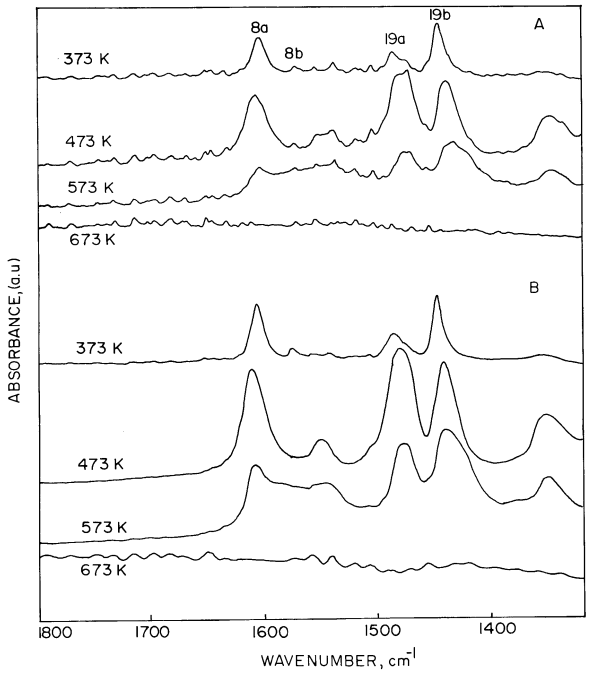

Fig. 8 Temperature dependent FTIR spectra of pyridine adsorbed on $CuFe_2O_4$ containing excess 0.5 mol CuO (A) or 0.5 mol Fe_2O_3 (B) between 373 K and 673 K. Note the increase in intensity and width of several features at high temperatures.

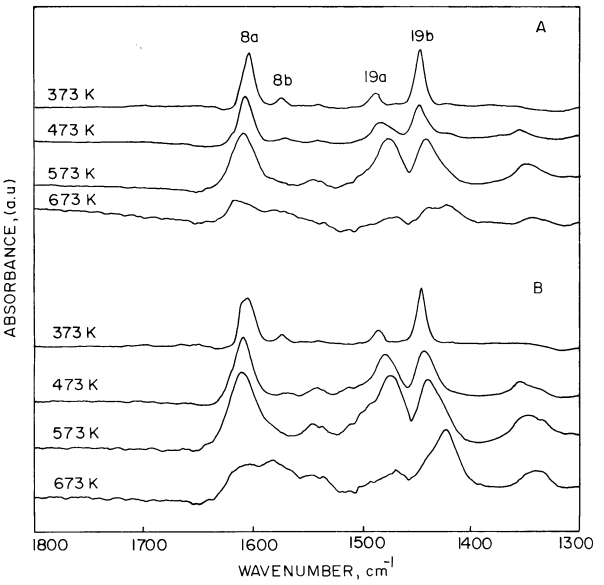

Fig. 9 Temperature dependent FTIR spectra of pyridine adsorbed on $CoFe_2O_4$ containing excess 0.5 mol CoO (A) or 0.5 mol Fe_2O_3 (B) between 373 K and 673 K. Note the stability of adsorbed pyridine even at 673 K.

Considering the polarizing power[12] and statistical distribution of cations, it can be assumed that, among these surface O_h sites, Fe^{3+} prevails over Co^{2+} and Cu^{2+} and consequently contributes more towards the pyridine adsorption and the imparting of Lewis acidity. This is further supported by increasing the Fe/(Cu + Co) surface atomic ratio from 0 to 1, calculated from XPS analysis (Table 1).[20] Nevertheless, Cu^{2+} and Co^{2+} indirectly influence the nature of surface active sites as follows. Upon pyridine adsorption there is electron flow from pyridine to the spinel surface resulting in the reduction of highly vulnerable cations, like Cu^{2+}, and the extent of reduction increases at high temperature. Consequently, the charge density around Fe^{3+} is also modified and leads to a decreased interaction between pyridine and the oxide surface and hence a less stable adsorbed complex. In contrast, Co^{2+} is robust and no reduction is observed on pyridine adsorption, even at high temperature. Hence Co^{2+} acts as a structure stabilizer and stabilizes the Fe^{3+} state in a higher proportion, probably exceeding the stoichiometric 1 : 2 ratio corresponding to the A and B sites in spinels. Thus Co^{2+} and Cu^{2+} ions affect the surface state of Fe^{3+} upon pyridine adsorption, in an exactly opposite manner. An increase in Co content decreases the reducibility of Fe^{3+} ions and consequently strengthens the Lewis acidity of ferrites. These results are further supported by our earlier studies with XPS, TPR and Mössbauer on $Cu_{1-x}Co_xFe_2O_4$.[19,20] Similar results were obtained from adsorption studies of n-butylamine followed by thermogravimetry by Ramankutty and Sugunan.[50]

Parallel to the above reported spectral changes, pyridine adsorption causes decreases in the intensity of various surface OH groups, seen as negative absorbance bands in the difference IR spectrum (Fig. 5). Since the pyridinium ion is simultaneously detected on all these samples, it is likely that the

reduction of the OH band intensity is due to the transfer of some protons from these OH groups to the adsorbed pyridine. Hydrogen bonded and bridged OH groups are expected to be less reactive than isolated terminal OH groups.[30] The large negative band observed at ~3720 cm^{-1} (Fig. 5) indicates that isolated OH groups bonded to Fe^{3+} and Co^{2+} ions are likely to be involved in pyridinium ion and α-pyridone formation. An increase in the intensity of the bands corresponding to pyridinium ion and α-pyridone with increasing temperature up to 473 K (Figs. 4 and 5) indicates that high temperature is essential to overcome the activation energy barrier for the formation of these species. Further, α-pyridone and bipyridyl formation is evident from the observation of a moderately intense band at 1352 cm^{-1} and unusual broadening of other bands with high intensity together with other minor features at high temperatures (Fig. 4). Such bipyridyl species are observed on semiconducting oxides such as Fe_2O_3 and SnO_2 and are formed *via* pyridine dimerization on heating.[51,52] The band observed at 1352 cm^{-1} corresponds to α-pyridone[53] and occurs through a nucleophilic attack of a surface OH group at ~3720 cm^{-1} on the 2-position of the aromatic ring.[53,54]

4.3. Basicity of $Cu_{1-x}Co_xFe_2O_4$

The formation of carbonate-like structures upon CO_2 adsorption reveals the surface basicity. Bicarbonate formation causes perturbation of the OH groups in the 3800–3500 cm^{-1} range and formation of certain new OH bands (not shown). Additionally, a weak band observed at 1220 cm^{-1} is attributed to the C–O–H bending vibration of bicarbonate.[43] Broad IR bands in the 1800–1200 cm^{-1} range indicate that bidentate species are predominant on the oxide surface due to CO_2 adsorption. On α-Al_2O_3[55] and MgO,[42,56] where the entire cationic coordination is due only to O_h, bidentates are, by far, the most prevalent structure. The large formation of bidentate carbonates indicates that the $Cu_{1-x}Co_xFe_2O_4$ surface possesses mainly O_h coordinated ions and reiterates our earlier conclusion.

Adsorption studies with EAs revealed that Cu-rich compositions possess a maximum number of strong basic sites that decreases considerably with increasing x. We propose that the basic strength of a surface oxide ion is stronger with more coordinative unsaturations and weaker with the greater polarising power of the cations to which it is bonded. The polarising power increases when there is an increase in charge and a decrease in size and *vice versa*. Strong or moderately strong basic sites would arise from structures where surface oxide ions bridge over two or more bivalent ions, while weak basic sites are expected on oxide ions bridging over Fe^{3+} ions. Also the O_h coordinated cation is larger than that of T_d and hence the polarizing power of the latter is higher than that of the former. Due to the above points, it is highly plausible that coordinatively unsaturated O_h cations, preferably divalent cations, offer strong basic sites and hence adsorbents like TCNQ, chloranil and CO_2 preferentially adsorb on these sites. It is reasonable to conclude that adsorption of an EA occurs mainly at the O_h sites. It is also clear that the O_h cation plays a significant role in determining the acid–base properties of the system. The extent of spinel inversion decreases with increasing x on $Cu_{1-x}Co_xFe_2O_4$ indicating that less divalent cations go to O_h sites and hence the basicity decreases with increasing x.

4.4. Acid–base strength and methylation activity performance

A detailed study on the performance of $Cu_{1-x}Co_xFe_2O_4$ catalysts in phenol methylation has already been reported.[20] Fig. 10 displays a comparison between the catalytic performance in terms of phenol conversion and selectivity to 2,6-xylenol obtained at a reaction temperature of 598 K with a

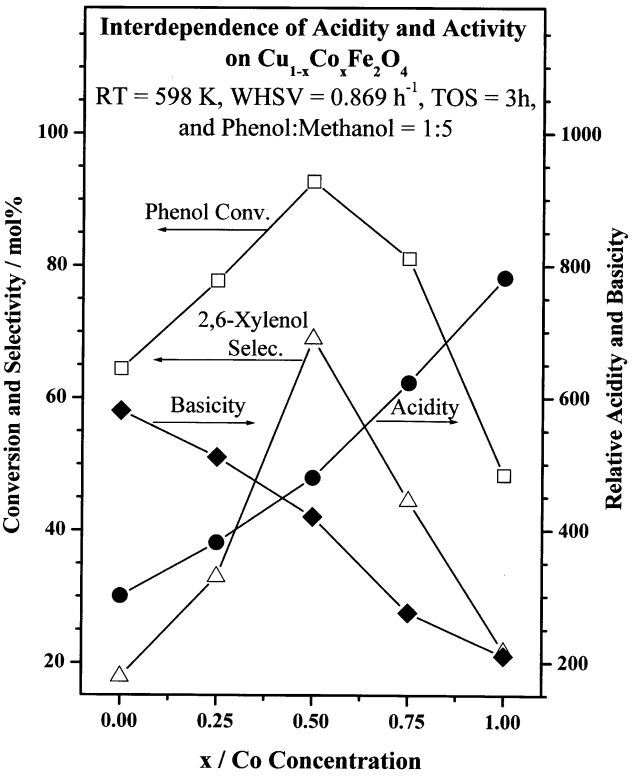

Fig. 10 A comparison between the catalytic performance (phenol conversion and selectivity of 2,6-xylenol), the relative acidity obtained from the area of the ν_{8a} and ν_{19b} bands from pyridine adsorbed on catalysts at 373 K and the relative basicity obtained from the area of the bands between 1700 and 1250 cm^{-1} from CO_2 adsorbed on $Cu_{1-x}Co_xFe_2O_4$ catalysts at 298 K. Note the good correlation between the intermediate acid–base property and high catalytic activity.

phenol:methanol feed composition of 1:5, and relative acidity (and basicity) obtained from the area of the ν_{8a} and ν_{19b} bands (bands between 1700 and 1200 cm^{-1}) in the FTIR spectra of pyridine (CO_2) adsorbed on the catalysts. Note that the Brønsted acid sites are not considered as they are too weak and the relative acidity and basicity given in Fig. 10 is qualitative. In this reaction methylation is sequential and 2,6-xylenol is produced at the expense of *o*-cresol; for simplicity *o*-cresol selectivity is not given in Fig. 10. A steep increase (decrease) in the relative acidity (basicity) with Co concentration (Fig. 10) clearly supports an increase (decrease) in acidity both in terms of strength and number. It is clear from Fig. 10 that neither the highly acidic (weakly basic) nor the weakly acidic (highly basic) catalyst at $x = 1.0$ and 0.0, respectively, is active for phenol conversion to 2,6-xylenol. However catalysts with $0.25 \geqslant x \leqslant 0.75$ show better catalytic performance and that with $x = 0.5$ is superior and demonstrates an intermediate acid–base character. This clearly indicates that an optimum acid–base property favours the overall reaction. It is also interesting to note that Friedel–Crafts alkylation reactions usually require highly acidic catalysts, which is not entirely true in the present case. The extent of the secondary methanol reforming reaction decreases from $x = 0$ to 1, as seen from the reduced Cu-species in the XPS results,[20] and this might explain the above contradiction. It is clear from Figs. 3, 7 and 10 that substitution of Co^{2+} for Cu^{2+} creates an increase in acidity with a concomitant decrease in the amount of basic sites. It has already been shown from earlier XPS results[20] on $Cu_{1-x}Co_xFe_2O_4$ that the $x = 0.5$ composition exhibits Cu–Co synergism which is correlated with the catalytic performance. Cu–Co synergism and low coke content at $x = 0.5$ among intermediate compositions[20] suggest that the intermediate acidity enhances the methylation activity by hydrogenation

of the coke to methyl species. This is further supported by the fact that the activity of Fischer–Tropsch catalyst is enhanced when Co is introduced into the system.[57]

5. Conclusions

A series of ferrospinels having the general composition $Cu_{1-x}Co_xFe_2O_4$ ($x = 0$, 0.25, 0.50, 0.75 and 1) was prepared by a co-precipitation method and characterized by FTIR for acid–base properties. The FTIR spectra of the ferrospinels reveal that Fe^{3+} and Co^{2+} ions are primarily responsible for the various OH groups between 3740 and 3620 cm^{-1}. Further, increasing x increases the number and strength of the OH groups. The FTIR spectrum of pyridine adsorbed on $Cu_{1-x}Co_xFe_2O_4$ surfaces at 373 K demonstrates that the predominant modes of adsorption are ν_{8a} and ν_{19b}, bolstering the dominant Lewis acid character. Pyridine adsorption on $Cu_{1-x}Co_xFe_2O_4$ and the deliberate addition of excess metal oxide to the spinel phase reveal that O_h coordinated ions are predominant on the surface and act as centers for pyridine adsorption; further, the contribution of various ions to the ν_{8a} band is in the following order $Fe^{3+} > Co^{2+} > Cu^{2+}$ in terms of its intensity and position. From the temperature dependent studies of pyridine adsorbed on surfaces of $Cu_{1-x}Co_xFe_2O_4$ and deliberately added excess oxide, it is clear that both Co^{2+} and Cu^{2+} ions influence the stability of the adsorbed pyridine complex in an opposite way to that in which Co^{2+} imparts stability to the surface. In general, the total intrinsic acidity of $Cu_{1-x}Co_xFe_2O_4$ increases with cobalt content. The formation of pyridinium ion also indicates the presence of Brønsted acidity, however it is weak.

CO_2 adsorption on $Cu_{1-x}Co_xFe_2O_4$ leads predominantly to the formation of the bidentate complex on the surface, which requires coordinatively unsaturated O_h ions on the surface. Adsorption studies of electron acceptors indicate that the basicity of the system decreases with increasing x. $CoFe_2O_4$ and $CuFe_2O_4$ show inverse trends in their acidic and basic behaviour and for $0.25 \geqslant x \leqslant 0.75$ there is some compromise between the acidic and basic behaviour. A good correlation exists between high catalytic activity and intermediate acid–base properties.

Acknowledgements

TM and NRS thank CSIR, New Delhi for the award of senior research fellowships. We thank Nisha and Sreeja Rani, Cochin University of Science and Technology, Cochin, for adsorption studies.

References

1 B. S. Rao, K. Sreekumar and T. M. Jyothi, *Indian Pat.*, 1998, 2707/98.
2 K. Sreekumar, T. Mathew, R. Rajagopal, R. Vetrivel and B. S. Rao, *Catal. Lett.*, 2000, **65**, 99.
3 K. Sreekumar, T. Mathew, B. M. Devassy, R. Rajagopal, R. Vetrivel and B. S. Rao, *Appl. Catal. A*, 2001, **205**, 11.
4 K. Sreekumar, T. Mathew, S. P. Mirajkar, S. Sugunan and B. S. Rao, *Appl. Catal. A*, 2000, **201**, L1.
5 B. S. Rao, T. Mathew, N. R. Shiju and R. Vetrivel, *Indian Pat.*, pending.
6 S. Ghorpade, V. S. Darshane and S. G. Dixit, *Appl. Catal. A*, 1998, **166**, 135.
7 P. S. Anilkumar, J. J. Shrotri, S. D. Kulkarni, C. E. Deshpande and S. K. Date, *Mater. Lett.*, 1996, **27**, 293.
8 M. C. Kung and H. H. Kung, *Catal. Rev. Sci. Eng.*, 1985, **27**, 425.
9 P. Berteau and B. Delmon, *Catal. Today*, 1989, **5**, 121.
10 G. Busca, *Catal. Today*, 1996, **27**, 323.
11 M. Rajendran, R. C. Pullar, A. K. Bhattacharya, D. Das, S. N. Chintalapudi and C. K. Majumdar, *J. Magn. Magn. Mater.*, 2001, **232**, 71.
12 G. Busca, *Catal. Today*, 1998, **41**, 191.
13 J. C. Lavalley, *Catal. Today*, 1996, **27**, 377.
14 G. Ramis, G. Busca and V. Lorenzelli, *Mater. Chem. Phys.*, 1991, **29**, 425.
15 R. Philipp and K. Fujimoto, *J. Phys. Chem.*, 1992, **96**, 9035.
16 S. Sugunan and G. D. Devika Rani, *Indian J. Chem.*, 993, **32**, A 1993.
17 S. Sugunan and G. D. Devika Rani, *J. Mater. Sci.*, 1993, **28**, 4811.
18 A. Auroux and S. Gervasini, *J. Phys. Chem.*, 1990, **94**, 6371.
19 K. Lázár, Z. Koppány, T. Mathew, J. Megyeri, V. Samuel, S. P. Mirajkar, B. S. Rao and L. Guczi, *Phys. Chem. Chem. Phys.*, 2002, **4**, 3530.
20 T. Mathew, N. R. Shiju, K. Sreekumar, B. S. Rao and C. S. Gopinath, *J. Catal.*, in press.
21 E. Prince and R. G. Treuting, *Acta Crystallogr.*, 1956, **9**, 1025.
22 J. Smith and H. P. J. Wijn, *Adv. Electron. Electron Phys.*, 1954, **6**, 83.
23 G. H. Jonker, *J. Phys. Chem. Solids*, 1959, **9**, 165.
24 N. F. M. Henry, J. Lipson and W. A. Wooster, *The Interpretation of X-Ray Diffraction Photographs*, Macmillan, London, 1951.
25 P. Tarte, *Spectrochim. Acta*, 1965, **19**, 49.
26 J. Preudhomma and P. Tarte, *Spectrochim. Acta, Part A*, 1971, **27**, 961.
27 R. D. Waldron, *Phys. Rev.*, 1955, **99**, 1727.
28 W. B. White and B. A. De Angelis, *Spectrochim. Acta, Part A*, 1967, **23**, 985.
29 G. Busca, V. Lorenzelli, G. Ramis and R. J. Willey, *Langmuir*, 1993, **9**, 1492.
30 C. H. Rochester and S. A. Topham, *J. Chem. Soc., Faraday Trans. 1*, 1979, **75**, 1073.
31 C. H. Rochester and S. A. Topham, *J. Chem. Soc., Faraday Trans. 1*, 1979, **75**, 1259.
32 G. Busca, V. Lorenzelli, V. S. Escribano and R. Guidetti, *J. Catal.*, 1991, **131**, 167.
33 G. Busca, V. Lorenzelli and V. Bolis, *Mater. Chem. Phys.*, 1992, **31**, 221.
34 G. Busca, R. Guidetti and V. Lorenzelli, *J. Chem. Soc., Faraday Trans.*, 1990, **86**, 989.
35 G. Busca, *J. Mol. Catal.*, 1987, **43**, 225.
36 C. H. Kline and J. Turkevich, *J. Chem. Phys.*, 1944, **12**, 300.
37 C. Morterra, A. Chiorino, G. Ghiotti and E. Garrone, *J. Chem. Soc., Faraday Trans. 1*, 1979, **75**, 271.
38 A. Ueno and C. O. Bennett, *J. Catal.*, 1978, **54**, 31.
39 G. Busca and V. Lorenzelli, *Mater. Chem.*, 1982, **7**, 89.
40 K. Nakamoto, *Infrared and Raman Spectra of Inorganic and Coordination Compounds*, 3rd edn., Wiley, New York, 1978, p. 243.
41 F. Solymosi and H. Knozinger, *J. Catal.*, 1990, **122**, 166.
42 C. Morterra, G. Ghiotti, F. Boccuzzi and S. Coluccia, *J. Catal.*, 1978, **51**, 299.
43 J. I. DiCosimo, V. K. Diez, M. Xu, E. Iglesia and C. R. Apesteguia, *J. Catal.*, 1998, **178**, 499.
44 G. Keresztury, M. Incze, F. Soti and L. Imre, *Spectrochim. Acta, Part A*, 1980, **36**, 1007.
45 R. P. Eischens and W. A. Pliskin, *Adv. Catal.*, 1952, **9**, 662.
46 D. M. Griffiths and C. H. Rochester, *J. Chem. Soc., Faraday Trans. 1*, 1977, **73**, 1988.
47 K. Esumi, H. Shimade and K. Meguro, *Bull. Chem. Soc. Jpn.*, 1977, **50**, 2795.
48 K. Esumi, K. Miyata, F. Waki and K. Meguro, *Bull. Chem. Soc. Jpn.*, 1986, **59**, 3363.
49 J. P. Jacobs, A. Maltha, J. R. H. Reintjes, T. Drimal, V. Ponec and H. H. Brogersma, *J. Catal.*, 1994, **147**, 294.
50 C. G. Ramankutty and S. Sugunan, *Appl. Catal. A*, 2001, **218**, 39.
51 G. Busca and V. Lorenzelli, *Mater. Chem.*, 1981, **6**, 175.
52 P. G. Harrison and E. W. Thornton, *J. Chem. Soc., Faraday Trans. 1*, 1975, **71**, 1013.
53 H. Knozinger, H. Krietenbrink, H. D. Muller and W. Schulz, in *Proceedings of the Sixth International Congress on Catalysis*, The Chemical Society, London, 1977, vol. 1, p. 183.
54 E. Borello, G. D. Gatta, B. Fubini, C. Morterra and G. Venturello, *J. Catal.*, 1974, **35**, 1.
55 C. Morterra, S. Coluccia, G. Ghiotti and A. Zecchina, *Z. Phys. Chem., Neue Folge*, 1977, **104**, 275.
56 J. V. Evans and T. D. Whately, *Trans. Faraday Soc.*, 1967, **63**, 2769.
57 G. Fornasari, A. D. Huysser, L. Mintcher, F. Trifiro and A. Vaccari, *J. Catal.*, 1992, **135**, 386.